International Journal of Electrical and Computer Engineering (IJECE)
Vol. 8, No. 2, April 2018, pp. 711 – 722
ISSN: 2088-8708, DOI: 10.11591/ijece.v8i2.pp711-722

Maximum Power Extraction Method for Doubly-fed Induction Generator Wind Turbine

Dinh Chung Phan and Trung Hieu Trinh
Faculty of Electrical Engineering, The University of Danang-University of Science and Technology, Vietnam

Article Info

Article history:
Received: Aug 11, 2017
Revised: Feb 23, 2018
Accepted: Mar 5, 2018

Keyword:
Doubly-fed induction generator
Lyapunov-function based controller
maximum available power
MPPT
Speed control
Wind turbine

ABSTRACT

This research presents a new scheme to extract the maximal available power from a wind turbine employing a doubly fed induction generator (DFIG). This scheme is developed from the wind turbine's MPPT-curve. Furthermore, we propose control laws for the rotor and grid side-converters. The stability of the proposed maximum available power method and the control laws are proved mathematically upon Lyapunov's stability criterion. Their efficiency is tested through the simulations of a DFIG wind turbine in Matlab/Simulink. Simulation results are analyzed and compared with that using a conventional scheme. Thanks to the suggested scheme, the wind turbine can track its maximum power point better and the electric energy output is higher comparing with that using the conventional scheme. Furthermore, by the suggested controllers, the rotor speed and current of the DFIG converged to their desired values. In other words, the wind turbine can achieve stable operations by the suggested control laws.

Corresponding Author:
Dinh Chung Phan
Faculty of Electrical Engineering, The University of Danang-University of Science and Technology
54-Nguyen Luong bang street, Lien Chieu district, Danang city, Vietnam
84-988983127
pdchung@dut.udn.vn

1. INTRODUCTION

The maximum power generation of a wind turbine has been interested in several decades and many algorithms have been suggested. According to [1], previous maximum power point tracking (MPPT) methods can be listed into three groups including indirect power controller, direct power controller, and others. The indirect power controller which aims to maximize mechanical power by using tip-speed ratio [2], [3], optimal torque [4], and power signal feedback MPPT algorithm [5] is simplicity and only allows the wind turbine to track its MPPT-curve quickly when a wind speed measurement is precise and instantaneous. In the case of an unavailable wind measurement, a wind turbine using the indirect power controller fails to track its maximum power point quickly and accurately [6], [7]. The direct power controller which maximizes electric power by using the perturbation and observation (P&O) algorithm such as: Hill climb search [8], incremental conductance [9], optimal-relation based MPPT algorithm [10], [11], and hybrid MPPT algorithm [12] does not require any wind turbine knowledge and available anemometer. Unfortunately, a wind turbine using the direct power controller cannot track its maximum power because this controller cannot recognize instantaneously the variation in wind speed. Until now, this controller has been implemented to adjust the voltage and current of DC circuit in a permanent magnetic synchronous generator wind turbine. The last group is developed based on soft computing techniques like Fuzzy [13] and Neural network [14]. A wind turbine using these methods only has a good performance when the full information of the wind turbine is available. However, these methods are complexity and large memory requirement. Hence, a new MPPT scheme for DFIG wind turbines should be researched.

To control the generator-wind turbine, proportional-integral (PI) control is normally implemented because of its simplicity [7], [15], [16]. However, by using the PI control, we cannot guarantee the wind turbine system will become stable operation [17], [18]. Recently, control laws based on sliding mode were suggested for rotor speed adjustment [19], [20]. However, these control laws require an available wind speed measurement. Hence, we need

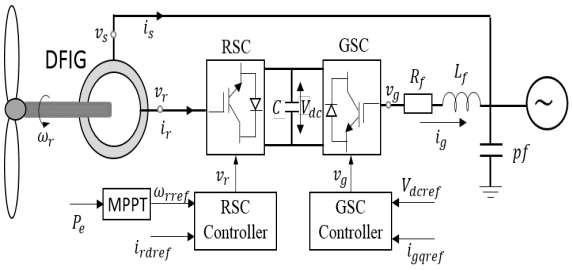

Fig. 1. DFIG wind turbine configuration

to propose a new control law for rotor speed in the DFIG-wind turbine.

In this research, we suggest a new scheme to extract the maximum available power from a wind turbine employing DFIG. This scheme is developed from the feedback power algorithm but in this research, we do not require an anemometer. New control laws which are developed upon Lyapunov function for rotor speed, current, and voltage are proposed. This scheme is validated through numerical simulations of a wind turbine employing DFIG. From simulation results, we will analyze and compare with the simulation results of a wind turbine using an old MPPT scheme.

2. DFIG WIND TURBINE

A DFIG-wind turbine is described in previous publications, as shown in Fig. 1. Generally, it consists of a wind turbine, shaft-gearbox, doubly-fed induction generator (DFIG), and back-to-back converter.

2.1. Wind turbine

When the wind turbine is rotating at a speed of ω_r and wind speed at the wind turbine is V_w, the mechanical power of the turbine is calculated through blade length R, air density ρ, and power coefficient $C_p(\lambda, \beta)$ [21]

$$P_m(t) \triangleq \frac{1}{2}\rho\pi R^2 C_p(\lambda,\beta)V_w^3(t). \tag{1}$$

The wind turbine's power coefficient $C_p(\lambda, \beta)$ depends on both pitch angle β and tip speed ratio λ [16]

$$\lambda(t) = \frac{R\omega_r(t)}{V_w(t)}. \tag{2}$$

At a constant λ, when β increases $C_p(\beta)$ will be decreased. In contrary, at a constant β, $C_P(\lambda)$ reaches to a maximum value $C_p(\lambda_{\rm opt})$ at $\lambda = \lambda_{\rm opt}$.

2.2. DFIG

The DFIG's main objective is to convert the mechanical power P_m on the wind turbine shaft to electricity power P_e. Relationship between P_e and P_m is described through the DFIG-wind turbine's inertia J

$$J\omega_r(t)\frac{\rm d}{{\rm d}t}\omega_r(t) = P_m(t) - P_e(t). \tag{3}$$

Generally, the DFIG is an induction generator so its rotor slip is defined as

$$s(t) \triangleq 1 - \frac{Np_n\omega_r(t)}{\omega_s}, \tag{4}$$

where p_n is the number of pole pairs; N is the gearbox ratio; ω_s is the rotational speed of stator flux.

In dq frame, the stator voltage $\mathbf{v}_s \triangleq \begin{bmatrix} v_{sd} & v_{sq}\end{bmatrix}^\top$ and rotor voltage $\mathbf{v}_r \triangleq \begin{bmatrix} v_{rd} & v_{rq}\end{bmatrix}^\top$ are computed from the stator current $\mathbf{i}_s \triangleq \begin{bmatrix} i_{sd} & i_{sq}\end{bmatrix}^\top$, rotor current $\mathbf{i}_r \triangleq \begin{bmatrix} i_{rd} & i_{rq}\end{bmatrix}^\top$, stator flux $\mathbf{\Psi}_s(t) = \begin{bmatrix}\Psi_{sd}(t) & \Psi_{sq}(t)\end{bmatrix}^\top$, rotor flux $\mathbf{\Psi}_r(t) = \begin{bmatrix}\Psi_{rd}(t) & \Psi_{rq}(t)\end{bmatrix}^\top$, rotor resistance r_r, rotor inductance L_r, stator resistance r_s, stator inductance

L_s, magnetizing inductance L_m as [22]

$$\begin{cases} \mathbf{v}_s(t) = r_s\mathbf{i}_s(t) + \omega_s\boldsymbol{\Theta}\boldsymbol{\Psi}_s(t) + \dfrac{\mathrm{d}}{\mathrm{d}t}\boldsymbol{\Psi}_s(t) \\ \mathbf{v}_r(t) = r_r\mathbf{i}_r(t) + s(t)\omega_s\boldsymbol{\Theta}(\boldsymbol{\Psi}_r(t) + \dfrac{\mathrm{d}}{\mathrm{d}t}\boldsymbol{\Psi}_r(t), \\ \boldsymbol{\Psi}_s(t) = L_s\mathbf{i}_s(t) + L_m\mathbf{i}_r(t) \\ \boldsymbol{\Psi}_r(t) = L_r\mathbf{i}_r(t) + L_m\mathbf{i}_s(t) \end{cases} \tag{5}$$

where $\boldsymbol{\Theta} \triangleq \begin{bmatrix} 0 & -1 \\ 1 & 0 \end{bmatrix}$.

Lemma 1. If we neglect the stator resistance, $r_s = 0$, and choose the dq frame so that $\boldsymbol{\Psi}_s(t) \equiv \begin{bmatrix} \Psi_{sd} & 0 \end{bmatrix}^\top$ then we can write the state-space equation of the DFIG (5) as

$$\frac{\mathrm{d}}{\mathrm{d}t}\mathbf{i}_r(t) = \mathbf{A}_r(t)\mathbf{i}_r(t) + \sigma^{-1}\mathbf{v}_r(t) + \mathbf{d}(t), \tag{6}$$

where

$$\sigma \triangleq L_r - \frac{L_m^2}{L_s},\ \ \mathbf{A}_r(t) \triangleq -\sigma^{-1}r_r\mathbf{I}_2 - \omega_s s(t)\boldsymbol{\Theta},\ \ \mathbf{d}(t) \triangleq -\frac{L_m}{\sigma L_s}s(t)\begin{bmatrix} 0 \\ V_s \end{bmatrix},\ \ \mathbf{I}_2 = \begin{bmatrix} 1 & 0 \\ 0 & 1 \end{bmatrix}. \tag{7}$$

Proof. Obviously, if we ensure $\boldsymbol{\Psi}_s(t) \equiv \begin{bmatrix} \Psi_{sd} & 0 \end{bmatrix}^\top$ then by using (5), we have

$$\boldsymbol{\Psi}_s(t) \quad = L_s\mathbf{i}_s(t) + L_m\mathbf{i}_r(t) = \begin{bmatrix} \Psi_{sd} & 0 \end{bmatrix}^\top,\ \ \frac{\mathrm{d}}{\mathrm{d}t}\boldsymbol{\Psi}_s(t) = 0 \Leftrightarrow L_s\frac{\mathrm{d}}{\mathrm{d}t}\mathbf{i}_s(t) = -L_m\frac{\mathrm{d}}{\mathrm{d}t}\mathbf{i}_r(t). \tag{8}$$

By using (8) and $r_s = 0$ in (5), we have

$$\mathbf{v}_s(t) = \omega_s\boldsymbol{\Theta}\boldsymbol{\Psi}_s(t) = \begin{bmatrix} 0 & \omega_s\Psi_{sd} \end{bmatrix}^\top = \begin{bmatrix} 0 & V_s \end{bmatrix}^\top, \tag{9}$$

where we used $V_s = \|\mathbf{v}_s(t)\| = |\omega_s\Psi_{sd}|$. From (8) and (9), we have

$$\mathbf{i}_s(t) = -\frac{L_m}{L_s}\mathbf{i}_r(t) + \frac{1}{L_s\omega_s}\begin{bmatrix} V_s \\ 0 \end{bmatrix},\quad \frac{\mathrm{d}}{\mathrm{d}t}\mathbf{i}_s(t) = -\frac{L_m}{L_s}\frac{\mathrm{d}}{\mathrm{d}t}\mathbf{i}_r(t). \tag{10}$$

From (10) and (5), we have

$$\boldsymbol{\Psi}_r(t) = \sigma\mathbf{i}_r(t) + \frac{L_m}{L_s\omega_s}\begin{bmatrix} V_s & 0 \end{bmatrix}^\top,\ \frac{\mathrm{d}}{\mathrm{d}t}\boldsymbol{\Psi}_r(t) = \sigma\frac{\mathrm{d}}{\mathrm{d}t}\mathbf{i}_r(t), \tag{11}$$

where we used $\sigma = L_r - L_m^2/L_s$. To use (11) and (5), we have

$$\mathbf{v}_r(t) = r_r\mathbf{i}_r(t) + \sigma\omega_s s(t)\boldsymbol{\Theta}\mathbf{i}_r(t) + \omega_s s(t)\Theta\frac{L_m}{L_s\omega_s}\begin{bmatrix} V_s & 0 \end{bmatrix}^\top + \sigma\frac{\mathrm{d}}{\mathrm{d}t}\mathbf{i}_r(t), \tag{12}$$

From (12), we can extract (6) easily. □

From [22] and by using (9) and (10), we calculate the stator side active power P_s in the DFIG as

$$P_s(t) = v_{sd}i_{sd} + v_{sq}i_{sq} = -\frac{L_m}{L_s}V_s i_{rq}(t). \tag{13}$$

2.3. Grid side converter

For the DFIG, the electricity frequency on the rotor side always depends on the rotor speed ω_r. Hence, to interface to the connected grid, a back to back converter which includes a rotor side converter(RSC), a DC-link, and a grid side converter (GSC) must be installed on the rotor side of the DFIG [23]. Normally, to reduce harmonic components generated by the GSC, a filter which consists of a resistor R_f, an inductor L_f in series and a power factor correction pf in parallel is used as Fig. 1.

In dq frame, the relationship of voltage $\mathbf{v}_g = \begin{bmatrix} v_{gd} & v_{gq} \end{bmatrix}^\top$ and current $\mathbf{i}_g = \begin{bmatrix} i_{gd} & i_{gq} \end{bmatrix}^\top$ of the GSC is written [24]

$$\frac{\mathrm{d}}{\mathrm{d}t}\mathbf{i}_g(t) = \mathbf{A}_g\mathbf{i}_g(t) + \mathbf{d}_g + \frac{1}{L_f}\mathbf{v}_g(t), \tag{14}$$

where

$$\mathbf{A}_g = -L_f^{-1}R_f\mathbf{I}_2 - \omega_s\mathbf{\Theta},\ \mathbf{d}_g = -L_f^{-1}\begin{bmatrix} V_s & 0 \end{bmatrix}^\top. \tag{15}$$

3. MAXIMUM WIND POWER EXTRACTION SCHEME

The optimal power control region of a wind turbine is limited by [25]

$$D \triangleq \{(\omega_r, V_w) \mid \omega_{r\min} \le \omega_r \le \omega_{r\mathrm{rated}}, V_{w\min} \le V_w \le V_{w\mathrm{rated}}, \beta = 0, \text{ and } C_p(\lambda,\beta) > 0\},$$

where $\omega_{r\min}$ and $\omega_{r\mathrm{rated}}$ are the minimum and rated rotor speed, respectively; $V_{w\min}$ and $V_{w\mathrm{rated}}$ stand for the minimum and rated wind speed; β is the blade system's pitch angle. Hence, when the wind turbine operates in D, the tip-speed ratio and the rotor speed reference are limited by

$$\lambda_{\min} \triangleq \frac{R\omega_{r\min}}{V_{w\mathrm{rated}}} \le \lambda(t) \le \lambda_{\max} \triangleq \max\{\lambda \mid C_p(\lambda,\beta) > 0\},$$
$$\omega_{r\min} \le \omega_{r\mathrm{ref}} \le \omega_{r\mathrm{rated}}.$$

From (1), to extract the maximization of the mechanical power, we must adjust ω_r to obtain the maximization of $C_p(\lambda(\omega_r, V_w))$. For any wind turbine, we have [24]

$$C_{p\max} \triangleq C_p(\lambda_{\mathrm{opt}}),\ \lambda_{\mathrm{opt}} \triangleq \arg\max_{\lambda} C_p(\lambda). \tag{16}$$

As the wind turbine operates at λ_{opt}, the rotor speed becomes the optimal rotor speed

$$\omega_{r\mathrm{opt}}(V_w) \triangleq \frac{\lambda_{\mathrm{opt}}V_w}{R} \tag{17}$$

and the mechanical power becomes maximal

$$\max_{\omega_r} P_m(\omega_r, V_w) = \frac{1}{2}\rho\pi R^2 C_{p\max}V_w^3 = k_{\mathrm{opt}}\omega_{r\mathrm{opt}}^3(V_w), \tag{18}$$

$$k_{\mathrm{opt}} \triangleq \frac{1}{2}\rho\pi R^5\frac{C_{p\max}}{\lambda_{\mathrm{opt}}^3}. \tag{19}$$

In this paper, the power coefficient in D is given as

$$C_p(\lambda) = \left(\frac{165.2842}{\lambda} - 16.8693\right)e^{-\frac{21}{\lambda}} + 0.009\lambda, \tag{20}$$

it has an unique maximum point of $C_{p\max} = 0.4$ at $\lambda_{\mathrm{opt}} = 6.7562$, and its mechanical power at different wind speed as shown in Fig. 2.

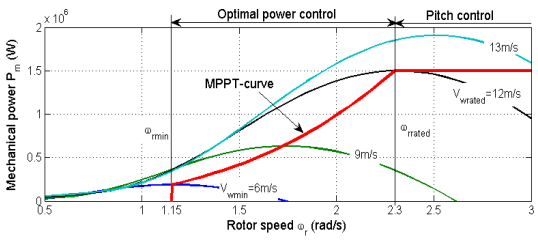

Fig. 2. MPPT curve of wind turbine

Remark 1. From (1), (2), and (19), we have [24]

$$P_m(t) - k_{\mathrm{opt}}\omega_r^3(t) = \zeta(t)\omega_r(t)(\omega_{r\mathrm{opt}}(t) - \omega_r(t)), \tag{21}$$

$$\zeta(\omega_r, V_w) = \pi\rho R^4\frac{V_w(t)}{2\lambda(t)}\frac{\frac{C_{p\max}}{\lambda_{\mathrm{opt}}^3}\lambda^3(t) - C_p(\lambda)}{\lambda(t) - \lambda_{\mathrm{opt}}} > 0. \tag{22}$$

3.1. Conventional MPPT-curve scheme

The conventional MPPT-curve method [7] makes

$$\omega_r \to \omega_{\rm rref} = \sqrt[3]{P_e/k_{\rm opt}}. \tag{23}$$

The problem is this conventional method cannot track quickly the maximum power point. Hence, we need to propose a new method as next subsection.

3.2. Proposal of maximum available power scheme

The subsection aims to propose a new scheme to maximize $P_m(\omega_r, V_w)$ or minimize the error $|\omega_{\rm ropt} - \omega_r(t)|$. To obtain this target, we propose $\omega_{ref}(t)$ satisfying

$$k_{opt}\omega^3_{rref}(t) = P_e(t) + \alpha k_{opt}(\omega^3_{rref}(t) - \omega^3_r(t)) + k\frac{\rm d}{{\rm d}t}\omega^2_r(t) + q^2(qy_{\rm max} - k\frac{\rm d}{{\rm d}t}\omega^2_r(t)) \tag{24}$$

where k, α, $y_{\rm max}$ are positive constants; and

$$q = \begin{cases} 0 \quad \text{for } |k\dfrac{\rm d}{{\rm d}t}\omega^2_r(t)| < y_{\rm max} \\ 1 \quad \text{for } k\dfrac{\rm d}{{\rm d}t}\omega^2_r(t) > y_{\rm max} \\ -1 \quad \text{for } k\dfrac{\rm d}{{\rm d}t}\omega^2_r(t) < -y_{\rm max}. \end{cases} \tag{25}$$

From (23) and (24), we can see that the proposed scheme is developed from the conventional MPPT method.

4. CONTROLLER DESIGN FOR DFIG

4.1. Rotor side control

The purpose of RSC controller is to reduce the errors $(i_{rd} - i_{rdref})$ and $(\omega_r - \omega_{\rm rref})$ in which i_{rdref} and $\omega_{\rm rref}$ are the reference of i_{rd} and ω_r, respectively. From (3), (6), (13), to make ω_r converge to $\omega_{\rm rref}$, we can adjust i_{rq} to a reference value i_{rqref} corresponding $\omega_{\rm rref}$. In [7], this task is carried by traditional PI controls. In this research, to obtain the above target, we design $\mathbf{v}_r$ of the DFIG (5) as

$$\mathbf{v}_r(t) = \mathbf{A}_r(t)\mathbf{i}_r(t) + \mathbf{d}(t) - \sigma\mathbf{K}_r\left(\mathbf{i}_{\rm rref}(t) - \mathbf{i}_r(t)\right) - \sigma\frac{\rm d}{{\rm d}t}\mathbf{i}_{\rm rref}(t), \tag{26}$$

$$\mathbf{i}_{\rm rref}(t) \triangleq \left[i_{rd\rm ref}(t) \quad i_{rq}(t) + k_{pr}e_{\omega_{\rm rref}}(t) + k_{ir}\int e_{\omega_{\rm rref}}(\tau)d\tau\right]^\top, \tag{27}$$

$$e_{\omega_{\rm rref}}(t) \triangleq \omega^3_{\rm rref}(t) - \omega^3_r(t), \tag{28}$$

where, $k_{pr} > 0$, $k_{ir} > 0$ and matrix $\mathbf{K}_r > 0$.

Theorem 1. When the DFIG-wind turbine operates in D, if $\omega_{\rm rref}$ and v_r of the DFIG (5) are designed as (24) and (26), respectively and if there exist positive constants μ_1, μ_2, and b satisfying

$$\min_D\left(2\zeta(t) - \frac{|\gamma(t)|}{\mu_1} - \frac{\xi(t)}{\mu_2}\right) > b\mu_1\hat{J}, \tag{29}$$

$$\min_D\left(2k_{ir} - \mu_2\xi(t) - \sqrt{\left[0 \quad 1\right]\mathbf{K}_r\mathbf{K}_r^\top\left[0 \quad 1\right]^\top}\right) > b\mu_1 k_{pr}, \tag{30}$$

$$\mathbf{K}_r + \mathbf{K}_r^\top - \sqrt{\mathbf{K}_r^\top\left[0 \quad 1\right]^\top\left[0 \quad 1\right]\mathbf{K}_r} > b\mu_1, \tag{31}$$

where

$$\hat{J} \triangleq J - 2k(1-q^2)),\ \gamma(t) \triangleq \hat{J}\frac{\rm d}{{\rm d}t}\omega_{\rm ropt}(t) - \hat{J}\frac{qy_{max}}{\omega_r(t)},\ \xi(t) \triangleq (1-\alpha)\frac{k_{\rm opt}}{\omega_r(t)},$$

then

$$\lim_{t\to\infty}\left(i_{\rm rref}(t) - i_r(t)\right) = 0,\ \lim_{t\to\infty}\left(\omega^3_{\rm rref}(t) - \omega^3_r(t)\right) = 0,\ |\omega_{\rm ropt} - \omega_r| \le \sqrt{\frac{\max_{\omega_r}|\gamma(t)|}{\hat{J}b}}.$$

Proof. Let define

$$\mathbf{e}_r(t) = \begin{bmatrix} e_{\omega_{\mathrm{rref}}}(t) & \mathbf{e}_{ir}(t) \end{bmatrix}^\top = \begin{bmatrix} \omega^3_{\mathrm{rref}}(t) - \omega^3_r(t) & \mathbf{i}_{rref}(t) - \mathbf{i}_r(t) \end{bmatrix}^\top$$
$$\mathbf{e}_m(t) = \begin{bmatrix} e_{\omega_{\mathrm{ropt}}}(t) & \mathbf{e}_r(t) \end{bmatrix}^\top = \begin{bmatrix} \omega_{opt}(t) - \omega_r(t) & \omega^3_{\mathrm{rref}}(t) - \omega^3_r(t) & \mathbf{i}_{rref}(t) - \mathbf{i}_r(t) \end{bmatrix}^\top.$$

By substituting (26) into (6), we have

$$\frac{\mathrm{d}}{\mathrm{d}t}\left(\mathbf{i}_{\mathrm{rref}}(t) - \mathbf{i}_r(t)\right) = -\mathbf{K}_r\left(\mathbf{i}_{\mathrm{rref}}(t) - \mathbf{i}_r(t)\right). \tag{32}$$

(27) can be rewritten as

$$k_{pr}\frac{\mathrm{d}}{\mathrm{d}t}e_{\omega_{\mathrm{rref}}}(t) = -k_{ir}e_{\omega_{\mathrm{rref}}}(t) + \begin{bmatrix} 0 & 1 \end{bmatrix}\frac{\mathrm{d}}{\mathrm{d}t}e_{ir}(t), \tag{33}$$

and by substituting (32) into (34), we have

$$k_{pr}\frac{\mathrm{d}}{\mathrm{d}t}e_{\omega_{\mathrm{rref}}}(t) = -k_{ir}e_{\omega_{\mathrm{rref}}}(t) - \begin{bmatrix} 0 & 1 \end{bmatrix}\mathbf{K}_r\mathbf{e}_{ir}(t), \tag{34}$$

Then,

$$\mathbf{E}_r\frac{\mathrm{d}}{\mathrm{d}t}\mathbf{e}_r(t) = -\mathbf{Q}_r\mathbf{e}_r(t), \tag{35}$$

$$\mathbf{E}_r = \begin{bmatrix} k_{pr} & 0 \\ 0 & I_2 \end{bmatrix} > 0, \;\; \mathbf{Q}_r = \begin{bmatrix} k_{ir} & \begin{bmatrix} 0 & 1 \end{bmatrix}\mathbf{K}_r \\ 0 & \mathbf{K}_r \end{bmatrix}. \tag{36}$$

When we define a Lyapunov function as $V_r \triangleq \mathbf{e}_r^\top(t)\mathbf{E}_r\mathbf{e}_r(t)$, its derivative is

$$\frac{\mathrm{d}}{\mathrm{d}t}V_r = \mathbf{e}_r^\top(t)\mathbf{E}_r\frac{\mathrm{d}}{\mathrm{d}t}\mathbf{e}_r(t) + \left(\frac{\mathrm{d}}{\mathrm{d}t}\mathbf{e}_r(t)\right)^\top\mathbf{E}_r\mathbf{e}_r(t). \tag{37}$$

By substituting (35) into (37), and noting that $\mathbf{Q}_r + \mathbf{Q}_r^\top = \tilde{\mathbf{Q}}_r$, we have

$$\frac{\mathrm{d}}{\mathrm{d}t}V_r = -\mathbf{e}_r^\top(t)\left(\mathbf{Q}_r + \mathbf{Q}_r^\top\right)\mathbf{e}_r(t) = -\mathbf{e}_r^\top(t)\tilde{\mathbf{Q}}_r\mathbf{e}_r(t) \le -\lambda_{\min}(\tilde{\mathbf{Q}}_r)\mathbf{e}_r^\top(t)\mathbf{e}_r(t). \tag{38}$$

Furthermore, by substituting (24) into (3)

$$\begin{aligned} J\omega_r(t)\frac{\mathrm{d}}{\mathrm{d}t}\omega_r(t) &= P_m(t) - k_{\mathrm{opt}}\omega^3_{\mathrm{rref}}(t) + \alpha k_{\mathrm{opt}}(\omega^3_{\mathrm{rref}}(t) - \omega^3_r(t)) + k\frac{\mathrm{d}}{\mathrm{d}t}\omega^2_r(t) + q^2(qy_{\max} - k\frac{\mathrm{d}}{\mathrm{d}t}\omega^2_r(t)) \\ &= P_m(t) - k_{\mathrm{opt}}\omega^3_r(t) + k_{\mathrm{opt}}(\omega^3_r(t) - \omega^3_{\mathrm{rref}}(t)) + k\frac{\mathrm{d}}{\mathrm{d}t}\omega^2_r(t) + \alpha k_{\mathrm{opt}}(\omega^3_{\mathrm{rref}}(t) - \omega^3_r(t)) \\ &+ q^2(qy_{\max} - k\frac{\mathrm{d}}{\mathrm{d}t}\omega^2_r) \\ &= \zeta(t)\omega_r(t)e_{\omega_{\mathrm{ropt}}}(t) + \xi(t)\omega_r(t)e_{\omega_{\mathrm{rref}}}(t) + q^3y_{\max} + 2k(1-q^2)\omega_r(t)\frac{\mathrm{d}}{\mathrm{d}t}\omega_r(t), \end{aligned} \tag{39}$$

where we use (21) and $(\alpha-1)k_{opt}(\omega^3_{\mathrm{rref}}(t) - \omega^3_r(t)) = \xi(t)\omega_r(t)(\omega_{\mathrm{rref}}(t) - \omega_r(t))$. By using $\hat{J} \triangleq J - 2k(1-q^2)$, (39) becomes

$$\hat{J}\frac{\mathrm{d}}{\mathrm{d}t}\omega_r(t) = \zeta(t)e_{\omega_{\mathrm{ropt}}}(t) + \xi(t)e_{\omega_{\mathrm{rref}}}(t) + \frac{q^3y_{max}}{\omega_r(t)}. \tag{40}$$

It means

$$\hat{J}\frac{\mathrm{d}}{\mathrm{d}t}e_{\omega_{\mathrm{ropt}}}(t) = -\zeta(t)e_{\omega_{\mathrm{ropt}}}(t) - \xi(t)e_{\omega_{\mathrm{rref}}}(t) \; + \gamma(t), \tag{41}$$

where we used $\gamma(t) = \hat{J}(\frac{\mathrm{d}}{\mathrm{d}t}\omega_{\mathrm{ropt}} - \frac{q^3y_{max}}{\omega_r(t)})$. Hence,

$$\mathbf{E}_m\frac{\mathrm{d}}{\mathrm{d}t}\mathbf{e}_m(t) = -\mathbf{Q}_m(t)\mathbf{e}_m(t) + \mathbf{M}_m(t) \tag{42}$$

where

$$\mathbf{E}_m = \begin{bmatrix} \hat{J} & 0_{1x3} \\ 0_{3x1} & \mathbf{E}_r \end{bmatrix},\ \mathbf{Q}_m(t) = \begin{bmatrix} \zeta(t) & \xi(t) & 0_{1x2} \\ 0 & k_{ir} & \begin{bmatrix} 0 & 1 \end{bmatrix} \mathbf{K}_r \\ 0_{2x1} & 0_{2x1} & \mathbf{K}_r \end{bmatrix},$$
$$\mathbf{M}_m(t) = \mathrm{diag}(\gamma(t), 0, 0, 0).$$

We define Lyapunov function as $V_m = \mathbf{e}_m(t)^\top \mathbf{E}_m \mathbf{e}_m(t)$, its derivative is

$$\frac{\mathrm{d}}{\mathrm{d}t} V_m = \mathbf{e}_m(t)^\top \mathbf{E}_m \frac{\mathrm{d}}{\mathrm{d}t} \mathbf{e}_m(t) + \left(\mathbf{E}_m \frac{\mathrm{d}}{\mathrm{d}t} \mathbf{e}_m(t) \right)^\top \mathbf{e}_m(t). \tag{43}$$

By using (42) in (43), we have

$$\frac{\mathrm{d}}{\mathrm{d}t} V_m = -\mathbf{e}_m(t)^\top \mathbf{Q}_m(t) \mathbf{e}_r(t) + \mathbf{e}_m(t)^\top \mathbf{M}_m(t) - \mathbf{e}_m(t)^\top \mathbf{Q}_m(t)^\top \mathbf{e}_m(t) + \mathbf{M}_m(t)^\top \mathbf{e}_m(t). \tag{44}$$

Noted that for $\mu_1 > 0$

$$\begin{aligned} \mathbf{e}_m(t)^\top \mathbf{M}_m(t) + \mathbf{M}_m(t)^\top \mathbf{e}_m(t) = 2 e_{\omega_{\mathrm{ropt}}}(t) \gamma(t) &\le e^2_{\omega_{\mathrm{ropt}}}(t) |\gamma(t)| / \mu_1 + \mu_1 |\gamma(t)| \\ &\le \mathbf{e}_m(t)^\top \mathbf{M}_{m1}(t) \mathbf{e}_m(t) + \mu_1 |\gamma(t)| \end{aligned} \tag{45}$$

where we used $\mathbf{M}_{m1}(t) = \mathrm{diag}(|\gamma(t)|/\mu_1, 0, 0, 0)$. Hence,

$$\frac{\mathrm{d}}{\mathrm{d}t} V_m \le -\mathbf{e}_m(t)^\top \tilde{\mathbf{Q}}_m(t) \mathbf{e}_m(t) + \mu_1 |\gamma(t)|, \tag{46}$$

where $\tilde{\mathbf{Q}}_m = \mathbf{Q}_m(t) + \mathbf{Q}_m(t)^\top - \mathbf{M}_{m1}(t)$.

Remark 2. For (29)-(31), with $\mu_2 > 0$, we have

$$\begin{aligned} \tilde{\mathbf{Q}}_m(t) &\ge \mathrm{diag}\left(2\zeta(t) - \frac{|\gamma(t)|}{\mu_1} - \frac{\xi(t)}{\mu_2}, 2k_{ir} - \mu_2 \xi(t) - \sqrt{\begin{bmatrix} 0 & 1 \end{bmatrix} \mathbf{K}_r \mathbf{K}_r^\top \begin{bmatrix} 0 \\ 1 \end{bmatrix}}, \mathbf{K}_r + \mathbf{K}_r^\top - \sqrt{\mathbf{K}_r^\top \begin{bmatrix} 0 \\ 1 \end{bmatrix} \begin{bmatrix} 0 & 1 \end{bmatrix} \mathbf{K}_r} \right) \\ &> b\mu_1 \mathbf{E}_m. \end{aligned}$$

and certainly, $\tilde{\mathbf{Q}}_r(t) > 0$.

Hence, according to the Lyapunov Stability Theory, (38) and (46) give us $\lim_{t\to\infty} \mathbf{e}_r(t) = 0$ and $|\omega_{\mathrm{ropt}} - \omega_r| \le \sqrt{V_m/\hat{J}} \le \sqrt{\max_{\omega_r} |\gamma(t)|/(\hat{J}b)}$. □

4.2. Grid-Side Control

In this section, we propose a new control law such that V_{dc} and i_{gq} are maintained at their references $V_{dc\mathrm{ref}}$ and $i_{gq\mathrm{ref}}$, respectively. To maintain V_{dc} at $V_{dc\mathrm{ref}}$, we need to make i_{gd} converge to $i_{gd\mathrm{ref}}$ corresponding to $V_{dc\mathrm{ref}}$.

Theorem 2. For any $V_{dc\mathrm{ref}}$ and $i_{gq\mathrm{ref}}$, if $\mathbf{v}_g$ of the GSC (14) are designed as

$$\mathbf{v}_g(t) = L_f \left(\frac{\mathrm{d}}{\mathrm{d}t} \mathbf{i}_{gr}(t) + \mathbf{K}_g \mathbf{e}_{ig}(t) - \mathbf{A}_g \mathbf{i}_g(t) \right) + \begin{bmatrix} V_s & 0 \end{bmatrix}^\top \tag{47}$$

$$\mathbf{i}_{gr}(t) = \begin{bmatrix} i_{gd}(t) + k_{pg} e_v(t) + k_{ig} \int e_v(\tau) d\tau & i_{gq\mathrm{ref}}(t) \end{bmatrix}^\top \tag{48}$$

$$e_v(t) = V^2_{dc\mathrm{ref}}(t) - V^2_{dc}(t),\ \mathbf{e}_{ig}(t) = \mathbf{i}_{gr}(t) - \mathbf{i}_g(t) \tag{49}$$

and if there exist $k_{pg} > 0$, $k_{ig} > 0$, and $\mathbf{K}_g > 0$ with

$$\tilde{\mathbf{Q}}_g = \begin{bmatrix} 2k_{ig} & \begin{bmatrix} 1 & 0 \end{bmatrix} \mathbf{K}_g \\ \mathbf{K}_g^\top \begin{bmatrix} 1 & 0 \end{bmatrix}^\top & \mathbf{K}_g^\top + \mathbf{K}_g \end{bmatrix} > 0, \tag{50}$$

then

$$\lim_{t\to\infty} (V^2_{dc\mathrm{ref}}(t) - V^2_{dc}(t)) = 0,\ \lim_{t\to\infty} (i_{gq\mathrm{ref}}(t) - i_{gq}(t)) = 0.$$

Proof. Let define $\mathbf{e}_g(t) = \begin{bmatrix} e_v(t) & \mathbf{e}_{ig}(t) \end{bmatrix}^\top$. By using (47) and (14), we have

$$\frac{\mathrm{d}}{\mathrm{d}t}\mathbf{e}_{ig}(t) = -\mathbf{K}_g\mathbf{e}_{ig}(t). \tag{51}$$

Furthermore, by taking time derivative of (48) and then using (51), we have

$$k_{pg}\frac{\mathrm{d}}{\mathrm{d}t}e_v(t) = -k_{ig}e_v(t) + \begin{bmatrix} 1 & 0 \end{bmatrix}\frac{\mathrm{d}}{\mathrm{d}t}\mathbf{e}_{ig}(t) = -k_{ig}e_v(t) - \begin{bmatrix} 1 & 0 \end{bmatrix}\mathbf{K}_g\mathbf{e}_{ig}(t). \tag{52}$$

Hence,

$$\mathbf{E}_g\frac{\mathrm{d}}{\mathrm{d}t}\mathbf{e}_g(t) = -\mathbf{Q}_g\mathbf{e}_g(t), \tag{53}$$

where

$$\mathbf{E}_g = \begin{bmatrix} k_{pg} & 0 \\ 0 & I_2 \end{bmatrix} > 0, \;\; \mathbf{Q}_g = \begin{bmatrix} k_{ig} & \begin{bmatrix} 1 & 0 \end{bmatrix}\mathbf{K}_g \\ 0 & \mathbf{K}_g \end{bmatrix}. \tag{54}$$

If we use a Lyapunov function as $V_g = \mathbf{e}_g(t)^\top\mathbf{E}_g\mathbf{e}_g(t)$, its time derivative will be

$$\frac{\mathrm{d}}{\mathrm{d}t}V_g = \mathbf{e}_g(t)^\top\mathbf{E}_g\frac{\mathrm{d}}{\mathrm{d}t}\mathbf{e}_g(t) + \left(\mathbf{E}_g\frac{\mathrm{d}}{\mathrm{d}t}\mathbf{e}_g(t)\right)^\top\mathbf{e}_g(t). \tag{55}$$

By substituting (53) into (55), we have

$$\frac{\mathrm{d}}{\mathrm{d}t}V_g = -\mathbf{e}_g(t)^\top\mathbf{Q}_g\mathbf{e}_g(t) - \mathbf{e}_g(t)^\top\mathbf{Q}_g^\top\mathbf{e}_g(t) = -\mathbf{e}_g(t)^\top\tilde{\mathbf{Q}}_g\mathbf{e}_g(t) \le -\lambda_{\min}(\tilde{\mathbf{Q}}_g)\mathbf{e}_g(t)^\top\mathbf{e}_g(t). \tag{56}$$

Hence, if (50) holds, then $\frac{\mathrm{d}}{\mathrm{d}t}V_g < 0$ for all nonzero $\mathbf{e}_g$. This completes the proof of Theorem 2. □

5. SIMULATION RESULT AND DISCUSSION

To evaluate the performance of the suggested MPPT scheme, we compare the simulation results of the 1.5 MW DFIG wind turbine with that using the conventional MPPT-curve scheme with traditional PI controls [7]. In this research, the generator and turbine parameters [22] as shown in Table 1 are used.

Table 1. Parameters of wind turbine and DFIG[22]

Name	Symbol	Value
Rated power	P	1.5 MW
The length of blade	R	35.25 m
Rated/minimum rotor speed	$\omega_{\mathrm{rrated}}/\omega_{r\min}$	22/11 rpm
Rated wind speed	$V_{w\mathrm{rated}}$	12 m/s
Rated stator voltage	V_s	690 V
Rated stator frequency	f	50 Hz
Number of pole pairs	p_n	2 p.u
Rotor winding resistance	r_r	2.63 mΩ
Stator winding inductance	L_s	5.6438 mH
Rotor winding inductance	L_r	5.6068 mH
Magnetizing inductance	L_m	5.4749 mH
Inertia of system	J	445 ton.m^2

With the power coefficient (20), the region D is

$$1.15 \le \omega_r \le 2.3, \;\; 1.15 \le \omega_{\mathrm{rref}} \le 2.3, \;\; 5 \le V_w \le 12, \;\; 3.4 = \lambda_{\min} \le \lambda \le 10.239.$$

In this region, $\zeta(\omega_r, V_w)$ as Fig. 3, which gives the minimum value ζ, $\min\zeta(\omega_r, V_w) = 1.271 \times 10^5$.

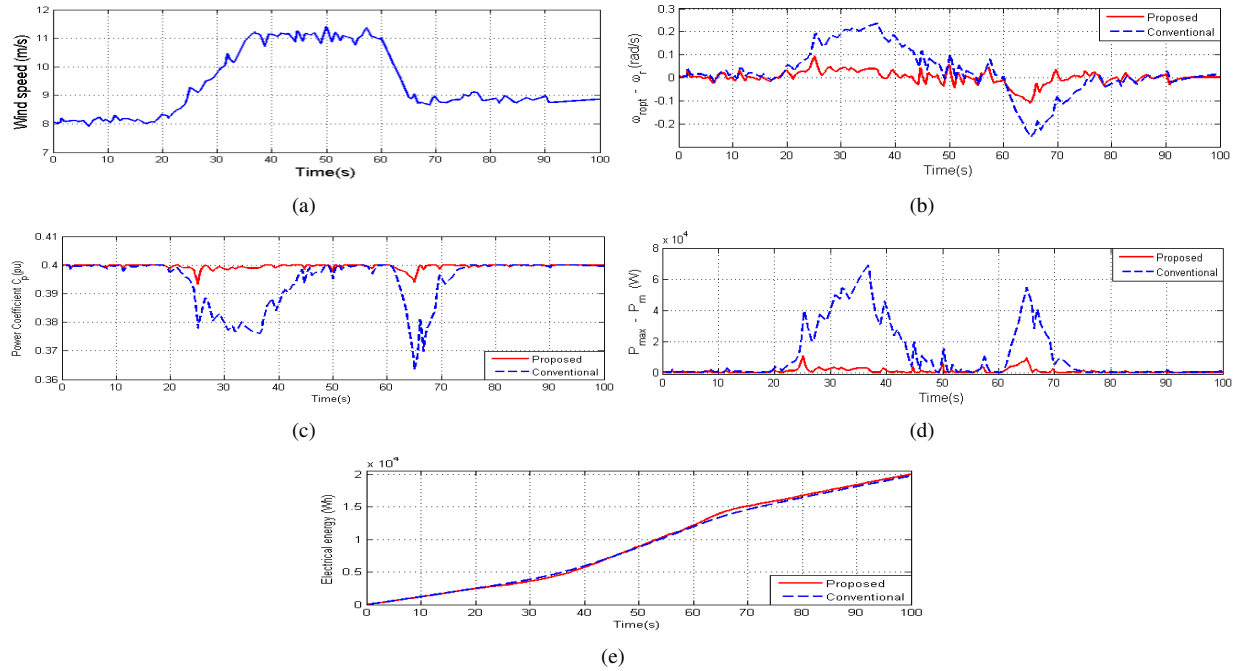

Fig. 4. Simulation results: (a) wind profile; (b) error between $\omega_{\rm ropt}$ and ω_r; (c) power coefficient C_p; (d) error between $P_{\rm max}$ and P_m; (e) electrical energy output

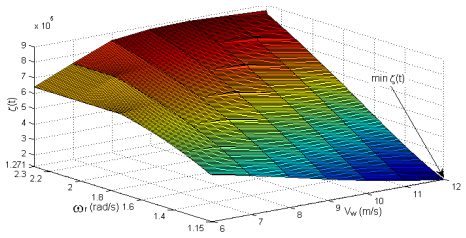

Fig. 3. $\zeta(\omega_r, V_w)$

Here, we use RSC controller's parameter as $k_{ir} = 0.4J$, $k_{pr} = 0.65J$, $\mathbf{K}_r = J\,\mathrm{diag}(0.5, 1)$, $k = 0.3J$, $\alpha = 0.2$, $y_{\max} = 0.1\omega_{\rm rrated}$.

For a wind profile with $\left|\frac{d}{dt}V_w\right| \leq 0.44m/s^2$, the boundary of $|\omega_{\rm ropt} - \omega_r|$ is determined as Table 2.

Table 2. Limitation of $|\omega_{\rm ropt} - \omega_r|$ as $\mu_1 = 1$ and $\mu_2 = 2$

Object	q=1	q=0
$\hat{J}$	4.45×10^5	3.12×10^5
$\max \xi(t)$	0.8673×10^5	0.8673×10^5
$\max \lvert\gamma(t)\rvert$	0.263 ×10^5	0.263
$b = 0.5915$	0.1895	0.5915
$\lvert\omega_{\rm ropt} - \omega_r\rvert$	1.2248rad/s	0.3775 rad/s

When the wind profile as Fig. 4a is used, simulation results are demonstrated in Fig. 4. Fig. 4b shows that when the wind speed has an insignificant change, the turbine speed is almost kept up at its optimal value. Since the wind turbine's large inertia, the turbine speed fails to respond instantaneously to the rapid change of the wind; this makes the turbine speed impossible to keep up at its optimal value. Therefore, the error $|\omega_{\rm ropt} - \omega_r|$ increases when the wind velocity changes rapidly. However, comparing with the turbine using the old MPPT scheme, by using the suggested scheme, the turbine speed can retain its optimal value more promptly because of the decrease in inertia from J to $(J - \alpha)$ and the error $|\omega_{\rm ropt} - \omega_r|$ is smaller. As a result, during a rapid change in wind conditions, in the

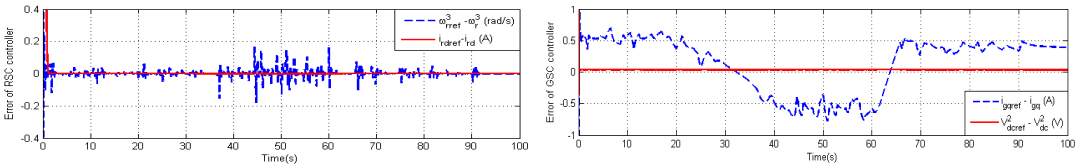

(a) (b)

Fig. 5. Error between reference signal and actual output in the controller: (a) errors of RSC controller and (b) errors of GSC controller

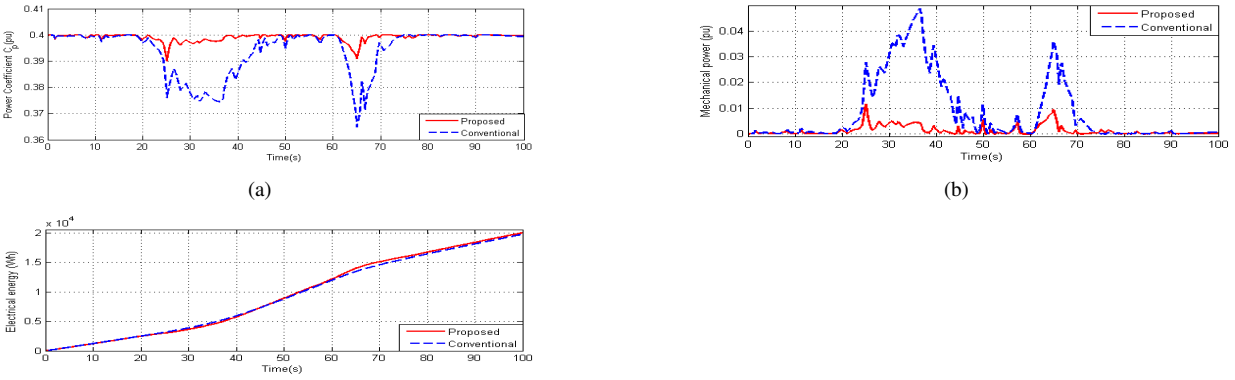

(a) (b)

(c)

Fig. 6. Simulation results with 5% measurement noise : (a) power coefficient; (b) error between $P_{\max}$ and P_m; (c) electrical energy output

proposed method, C_p restores $C_{p\max}$ more quickly, as shown in Fig. 4c. Obviously, by implementing the old MPPT scheme, the C_p can be reduced to to 0.363 while by implementing the proposed scheme, this data is 0.393.

Figure 4d shows the efficiency of the suggested method comparing with the conventional one in terms of mechanical power. When the wind velocity varies insignificantly, the error $(P_{\max} - P_m)$ in the wind turbine using the suggested scheme is like that using the conventional one. However, this error becomes significant when the wind changes suddenly; by using the new method this error is significant smaller comparing with that using the old one thanks to the restoration of C_p.

Fig. 4e indicates that to increase the turbine velocity in the period of 20s-40s, the turbine using the offered scheme requires a higher mechanical power comparing with that using the old one. However, the stored mechanical power is returned in the interval of 60s-75s in which the rotor speed decreases. Hence, in the period of 20s-40s, comparing with the DFIG using the suggested scheme, the electric energy generated by the DFIG using the old MPPT method is little higher but in the 60s-75s interval, it becomes opposite. As a result, accumulating to the end of simulation, the wind turbine using the conventional method fails to generate the electrical energy in total as high as that using the proposed method, as Fig. 4e. This indicates the quality of the suggested MPPT scheme.

Fig. 5 shows the control quality of the RSC and GSC. Both $(\omega_{\text{rref}}^3 - \omega_r^3)$ and $(i_{rd\text{ref}} - i_{rd})$ in Fig. 5a are very small, it means ω_r and i_{rd} track their reference values; in other words, the control law proposing for the RSC has a good performance. Likely, from Fig. 5b, the errors of $(V_{d\text{cref}}^2 - V_{dc}^2)$ and $(i_{gq\text{ref}} - i_{gq})$ are about zero; in other words, the controller suggesting for the GSC has a qualified performance.

When a measurement noise, 5% of rated values, is added to the measurement signals, $\mathbf{i}$, ω_r, with the wind profile as Fig. 4a, the simulation results are shown in Fig. 6. This figure indicates that with the above noise measurement, the turbine using the recommended MPPT scheme still tracks its maximum points more exactly comparing with the turbine using the old MPPT scheme. However, comparing with the case of pure measurement as Fig. 4, the measurement noise causes a negative impact on the turbine performance but this impact is insignificant.

Fig. 7 is the simulation results for a wind profile which varies rapidly as Fig. 7a. It is easy to see from Fig. 7b and Fig. 7c that the turbine using the suggested scheme has more qualified performance in both the power coefficient C_p and the electrical energy in total comparing with the case using the conventional scheme.

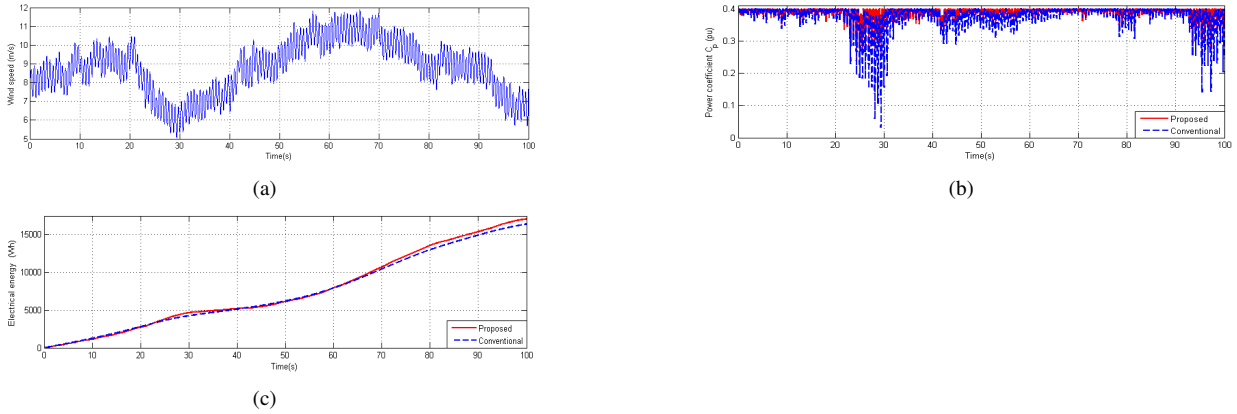

Fig. 7. Simulation results in the case of rapidly-varying wind velocity: (a) wind profile; (b) power coefficient; (c) electrical energy output

6. CONCLUSIONS

This paper suggested a new MPPT scheme for variable speed wind turbines using a DFIG. The suggested scheme allows the turbine tracking the maximum-power-point more effectively than the turbine using the MPPT-curve scheme. As can be seen from the simulation results, by using the suggested scheme, C_p almost keeps up $C_{p\max}$, ω_r was approximate to $\omega_{\rm ropt}$ and the electric energy generated by the DFIG was higher comparing with that using the conventional scheme. Furthermore, by the suggested controllers, the rotor speed and current of the DFIG converged to their desired values. Thus, by the suggested control law, the wind turbine can achieve stable operations.

REFERENCES

[1] D. Kumar, et al., "A review of conventional and advanced MPPT algorithms for wind energy systems," *Renewable and Sustainable Eneergy Review*, vol. 55, pp. 957-970, 2016.

[2] D. V. N. Ananth, G. V. Nagesh Kumar, "Tip speed ratio based MPPT algorithm and improved field oriented control for extracting optimal real power and independent reactive power control for grid connected doubly fed induction generator," *International Journal of Electrical and Computer Engineering*, vol. 6, no. 3, pp.1319- 1331, 2016.

[3] S. Rajendran, et al., "Variable speed wind turbine for maximum power capture using adaptive fuzzy integral sliding mode control," *Journal of Modern Power System and Clean Energy*, 2(2), pp. 114-125, 2014.

[4] M. Nasiri, et al., "Modeling, analysis and comparison of TSR and OTC methods for MPPT and power smoothing in permanent magnet synchronous generator-based wind turbines," *Energy Conversion Managment*, vol. 86, pp. 892-900, 2014.

[5] Q. Wang Q, et al., "An intelligent maximum power extraction algorithm for inverter-based variable speed wind turbine systems," *IEEE Trans Power Electron*, vol. 19(5), pp. 1242-1249, 2004.

[6] R. Sarrias-Menaa, et al., "Fuzzy logic based power management strategy of a multi-MW doubly-fed induction generator wind turbine with battery and ultracapacitor," *Energy*, vol. 70, pp. 561-576, 2014.

[7] L. Fernandez, et al., "Comparative study on the performance of control systems for doubly fed induction generator (DFIG) wind turbines operating with power regulation," *Energy*, vol. 33(9), pp. 1438-1452, 2008.

[8] M. Abdullah, et al., "A review of maximum power point tracking algorithms for wind energy systems," *Renewable and Sustainable Energy Review*, vol. 16(5), pp. 3220-3227, 2012.

[9] K. N. Yu, et al, "Applying novel fractional order incremental conductance algorithm to design and study the maximum power tracking of small wind power systems," *Journal of Applied Research and Technology*, vol. 13, pp. 238-244, 2015.

[10] Y. Xia, et al., "Wind turbine power coefficient analysis of a new maximum power point tracking technique," *IEEE Transaction on Industrial Electronic*, vol. 60(3), pp. 1122-1132, 2013.

[11] H. B. Zhang, et al., "One-power-point operation for variable speed wind/tidal stream turbines with synchronous generators," *IET Renewable Power Generation*, vol. 5(1), pp. 99-108, 2011.

[12] Y. Xia, et al., "A new maximum power point tracking technique for permanent magnet synchronous generator based wind energy conversion system," *IEEE Transaction on Power Electronic*, vol. 26(12), pp. 3609-3620, 2011.

[13] V. Calderaro, et al., "A fuzzy controller for maximum energy extraction from variable speed wind power generation systems," *Electric Power System Research*, vo. 78(6), pp. 1109-1118, 2008.
[14] R. Ata, "Artificial neural networks applications in wind energy systems: a review," *Renewable and Sustainable Energy Revew*, vol. 49, pp. 534-562, 2015.
[15] Anju M1, R. Rajasekaran, "Power system stability enhancement and improvement of LVRT capability of a DFIG based wind power system by using SMES and SFCL," *International Journal of Electrical and Computer Engineering*, vol. 3, no. 5, pp.618-628, 2013.
[16] Naim Cherfia, Djallel Kerdoun, "Wind energy conversion systems based on a DFIG controlled by indirect vector using PWM and SVM," *International Journal of Electrical and Computer Engineering*, vol. 6, no. 2, pp.549-559, 2016.
[17] L. Yang, et al., "Oscillatory stability and eigenvalue sensitivity analysis of a DFIG wind turbine system," *IEEE Transaction on Energy Conversion*, vol.26(1), pp. 328-339, 2011.
[18] Y. Mishra, et al., "Small signal stability analysis of a DFIG-based wind power system under different modes of operation," *IEEE Transaction on Energy Conversion*, vol. 24(4), pp. 972-982, 2009.
[19] O. Barambones O, et al., "Robust speed control for variable speed wind turbine," *International Journal of Innovation Computer, Information and Control*, vol. 8(11), pp. 7627-7640, 2012.
[20] W. Lin W, et al., "On-line designed hybrid controller with adaptive observer for variable-speed wind generation system," *Energy*, vol. 35(7), pp. 3022-3030, 2010.
[21] Bineeta Mukhopadhyay, at al., "Voltage compensation in wind power system using STATCOM controlled by soft computing techniques," *International Journal of Electrical and Computer Engineering*, vol. 7, no. 2, pp.667-680, 2017.
[22] B. Wu B, et al., "Power conversion and control of wind energy system," Hoboken, New Jersey: John Wiley & Sons, 2011.
[23] G. Venu Madhav, Y. P. Obulesu, "A new hybrid artificial neural network based control of doubly fed induction generator," *International Journal of Electrical and Computer Engineering*, vol. 5, no. 3, pp.379 390, 2015.
[24] D. C. Phan DC and S. Yamamoto, "Maximum Energy Output of a DFIG Wind Turbine Using an Improved MPPT-Curve Method," *Energies*, vol. 8, pp. 11718-11736, 2015.
[25] D. C. Phan DC and S. Yamamoto, "Rotor speed control of doubly fed induction generator wind turbines using adaptive maximum power point tracking," *Energy*, vol. 111, pp. 377-388, 2016.

BIOGRAPHIES OF AUTHORS

Dinh Chung Phan has been a lecture at Faculty of Electrical engineering, The university of Danang-University of Science and Technology in Vietnam since 2004. He obtained Engineering Degree, Master Degree and Philosophy Degree in electrical engineering from The university of Danang-University of Science and Technology in 2004, Dongguk university in Korea in 2011, and Kanazawa university in Japan in 2017, respectively. His researches are in fields of renewable energy, power system and control. Further info on his homepage: http://scv.udn.vn/phandinhchung

Trung Hieu Trinh has been a lecture at Faculty of Electrical engineering, The university of Danang-University of Science and Technology, in Vietnam since 2006. He obtained Engineering Degree and Philosophy Degree in electrical engineering from Hanoi University of Science and Technology in Vietnam in 2006 and Grenoble Institut of Technology in France in 2013, respectively. His researches are in fields of renewable energy, power electronic, and high voltage technology. Further info on his homepage: http://scv.udn.vn/tthieu